First-principles study of the effect of pressure on the five zirconia polymorphs. I. Structural, vibrational, and thermoelastic properties

Giuseppe Fadda,[1,2,*] Giovanni Zanzotto,[1,†] and Luciano Colombo[2,‡]

[1]*Dipartimento di Metodi e Modelli Matematici per le Scienze Applicate, Università degli Studi di Padova, Via Trieste, 63, I-35121 Padova (PD), Italy*

[2]*Dipartimento di Fisica, Università degli Studi di Cagliari–Cittadella Universitaria, I-09042 Monserrato (Cagliari), Italy*

(Received 19 April 2010; published 17 August 2010)

The structural parameters and phonon spectra of the five known polymorphs of zirconia are computed for pressures up to 48 GPa with density-functional perturbation theory within both the local-density and the generalized gradient approximations. Thermoelastic properties in the quasiharmonic approximation, including Grüneisen mode parameters (Part I), and dielectric properties, including the lattice contribution and the Raman spectra (Part II) are derived from the phonon calculations and compared to results of experiments and previous computations.

DOI: 10.1103/PhysRevB.82.064105 PACS number(s): 62.50.−p, 63.20.dk, 64.70.K−, 65.40.−b

I. INTRODUCTION

Zirconia (zirconium dioxide ZrO_2) is a highly versatile material having excellent mechanical, thermal, chemical, and dielectric properties; it has therefore found many technological applications, such as high-temperature fuel cells, nuclear-waste confinement, bone prosthetics, ceramics toughening, and microelectronics (see Refs. 1–10 and references therein).

Zirconia exists under five different forms which have been fully characterized crystallographically. The monoclinic (baddeleyite $P2_1/c$, below 1500 K), tetragonal $P4_2/nmc$ (between 1500 and 2650 K), and cubic $Fm\bar{3}m$ (isostructural to fluorite CaF_2, above 2650 K) polymorphs are stable at room pressure whereas the two orthorhombic *Pbca* and *Pnma* polymorphs (respectively, isostructural to brookite TiO_2 and to cotunnite $PbCl_2$) are stable between 3–5 GPa and 12.5–20 GPa and above 12.5–20 GPa, respectively.[11–17]

The structural, thermoelastic, vibrational, and dielectric properties of the most common zirconia polymorphs at room pressure have been investigated through first-principles methods in Refs. 6 and 18–21 for the cubic, tetragonal, and monoclinic ZrO_2 phases. A recent study[22] has investigated such properties in the tetragonal phase under varying hydrostatic pressure, up to 40 GPa; see also Refs. 23 and 24 and references therein for the structural and elastic properties of the zirconia polymorphs at room pressure. The present work is devoted to a reassessment and extension of such previous analyses together with the first *ab initio* investigation of the vibrational and dielectric properties of the two high-pressure orthorhombic phases (an earlier computation concerning the orthorhombic *Pnma* phase, Ref. 25, was based on an empirical force model). For these purposes, we have employed density-functional theory in both the local-density (LDA) and the generalized gradient approximations (GGA) for the pseudopotentials, and we have performed our study under pressure up to 48 GPa. Based on the results so obtained on phonons, we have derived in the present paper (hereafter referred to as Part I), within the quasiharmonic approximation, several observable thermoelastic quantities on which experimental and computational information are available. The dielectric properties and their pressure dependence are, in turn, investigated in a second paper[26] (indicated as Part II).

We find that ZrO_2 has generally positive Grüneisen parameters (see below), and that the GGA leads to a systematic non-negligible underestimate of the phonon frequencies,[27–29] and consequently to a noticeable overestimate of the dielectric constants. Nonetheless, we obtain good agreement of either the GGA or LDA results when matched to different, partially contradictory, experimental data on thermoelastic properties. Only the LDA results agree, however, with previously published data for the dielectric behavior (Part II). The complete set of structural, vibrational, dielectric, and thermoelastic quantities presently computed may aid future experimental work on these five ZrO_2 phases.

This paper is organized as follows: after a description of the computational setup in Sec. II, the structural parameters and their pressure dependence are given in Sec. III, wherein are discussed also the zirconia transitions at 0 K. The phonon spectra at 0 K of the five known polymorphs are computed under varying pressure in Sec. IV. In Sec. V we discuss some thermoelastic properties computed within the quasiharmonic approximation (heat capacities, thermal expansion, and bulk modulus). Some conclusions are presented in Sec. VI.

II. COMPUTATIONAL DETAILS

A. Pseudopotentials

Hartree atomic units are used throughout. The QUANTUM-ESPRESSO package[30] was used to perform all computations. Two sets of pseudopotentials are used in the following; both are based on all-electron scalar-relativistic computations and were built using the Vanderbilt ultrasoft scheme.[31]

1. GGA set

The first set of potentials is the PAW set used in Ref. 23. The exchange-correlation functional is the one by Perdew, Burke, and Ernzerhof.[32]

For zirconium, the fourth and fifth shell electrons are all considered valence electrons; the cutoff radii are 1.8 a.u., 2.0 a.u., and 2.2 a.u. for the *s*, *p*, and *d* subshells, respectively. Nonlinear partial core corrections[33] are included. For oxy-

gen, the valence electrons are those of the second shell; the cutoff radius is 1.1 a.u. for both s and p subshells.

2. LDA set

The second set of Vanderbilt ultrasoft potentials is based on the Perdew-Zunger parametrization[34] of the Ceperley-Alder computations of the electron gas.[35] The potentials are taken without modifications from Vanderbilt's USPP package.[36]

For zirconium, the valence electrons are $4s^2 4p^6 4d^1 5s^2$ (note that the valence electrons are $s^2 d^1$ instead of $s^2 d^2$ as above) with cutoff radii of 1.8 a.u., 1.8 a.u., and 1.7 a.u. for the s, p, and d subshells, respectively. There are no core corrections. The choice of valence electrons is the same as above for oxygen with cutoff radii of 1.3 a.u. for both subshells.

3. Sampling, cutoff energy, and convergence

The Brillouin zone (BZ) is sampled using the Monkhorst-Pack scheme[37] with (unless otherwise stated) a $4\times4\times4$ grid for all phases and a cutoff energy of the plane-wave expansion fixed at $E_{\text{cut}}=15$ Ha.

Convergence studies are practical for the cubic and tetragonal phases only; a good measure of convergence (for the properties analyzed in Part I) is the value of the phonon frequencies for the paths illustrated in the following. For both phases, computations were done for the nominal $4\times4\times4$ grid with $E_{\text{cut}}=15$ Ha and for a $8\times8\times8$ grid with $E_{\text{cut}}=30$ Ha. The root mean squares of the relative errors were found to be 25.2% and 8.62% (GGA) and 2.83% and 0.396% (LDA), respectively; it appears that the bulk of the errors is in the three lowest branches, as indeed the root mean squares drop without them to 0.927 and 4.86% (GGA) and 0.165 and 0.330% (LDA). In the cubic case another difficulty is created by the unstable dispersion branch along the Γ-X-W direction (see below). Because of this instability, we have not included any results for the cubic phase derived from the phonon density of states (DOS).

An intermediate GGA computation with the nominal $4\times4\times4$ grid but $E_{\text{cut}}=30$ Ha gives for all branches a difference, with respect to the $8\times8\times8$ computation, of 0.385% and 2.93% for the cubic and tetragonal cases, respectively, which seems to indicate that the source of divergence is the energy cutoff.

The combination of a $4\times4\times4$ grid and a cutoff energy of 15 Ha seems therefore an appropriate trade-off in the LDA case (but apparently less so in the GGA case) of reasonable precision and computational speed-up, much needed given the fairly large load required by first-principles phonon calculations for the ZrO_2 structures considered in this work.

As to the dielectric properties, between the results obtained with a $8\times8\times8$ grid and $E_{\text{cut}}=30$ Ha and the nominal sampling, the relative errors for all components of the electronic and lattice contributions are within 3% except for the $\epsilon_{11}^{\text{lattice}}$ component of the tetragonal phase (GGA, 8.10%, see Part II).

4. LDA and GGA pseudopotentials

It is known that, with respect to the corresponding LDA computations, elastic parameters computed with the GGA pseudopotentials are underestimated (compare Refs. 23 and 38 with Refs. 39 and 40; see also Ref. 41 for another class of materials), structural parameters being conversely overestimated (see Refs. 41 and 42 and Table I of the present work for a comparative study on zirconia); also well documented is the tendency of the GGA pseudopotentials to soften phonons.[27–29] This comes from the fact that the generalized gradient approximation acts as a negative pressure field by reduction, with respect to the local-density approximation, of the capacity of the valence electrons to screen the ion-ion interactions;[27,43] thus, as Grüneisen parameters are generally positive (see Sec. II C 3 below), an increase in equilibrium volume means a decrease in the phonon frequencies.

With the exception of Ref. 29, which, exactly as with the present GGA computations, underestimates the frequencies, all other published results have been obtained with LDA pseudopotentials. The same large difference on frequencies between GGA and LDA potentials was observed with hafnium oxide HfO_2 (see Ref. 28), which shares many structural similarities with zirconia.[44]

B. Computation of the phonon spectra

The computation of the vibrational properties by QUANTUM-ESPRESSO follows the theoretical framework of Ref. 45, based on density-functional perturbation theory. The phonon dispersion curves are computed by interpolation of the force constants.[45]

The longitudinal optic (LO)-transversal optic (TO) splitting is a consequence of the ionic displacements, which, at the long-wavelength limit, generate dipoles and thus a macroscopic electric field; it is taken into account through the computation of a nonanalytic term including the Born effective charges, see Ref. 46 for details. The LO frequencies at the $k\rightarrow0$ limit are direction-dependent (except for the cubic crystallographic system), which shows in the phonon dispersion curve under the form of discontinuities at the Γ point.

The vibrational DOS is computed with the tetrahedron method,[47,48] as implemented in QUANTUM-ESPRESSO; the calculation of partial DOS has been added to the original code. The weight of each crystallographic orbit (i.e., the subset of atoms in the crystal whose positions are related by an operation in the space group) is, for each phonon branch and each sample point in the BZ, the relative sum of the norms of the polarization vectors of the atoms belonging to that orbit; no smoothing has been applied. The density of states has been normalized to 1 in order to compare the various phases.

C. Quasiharmonic approximation and Grüneisen parameters

1. Methodology

We follow standard treatments, see, for instance, Refs. 49–54. In the quasiharmonic approximation, the phonon density of states only depends on the volume V, the temperature dependence being taken into account indirectly through V. The phonon spectra are first computed for a number of equilibrium volumes V_i (each corresponding to a different pressure); the thermodynamic potential $F(V_i, T_j)$ at various tem-

TABLE I. Computed structural parameters, at $p=0$, of the known polymorphs of zirconia; see Ref. 23 for details and a summary of the published results. The space group is indicated on the leftmost column, the lattice parameters in the middle column, the Wyckoff positions (Ref. 58) with the value of the free parameters (contravariant coordinates), on the right. Origin choice 2 was taken for the tetragonal polymorph. The orbit labeling indicated here is used in the following figures.

Phase	Lattice parameters	Crystallographic orbits and parameters		
GGA (15 Ha)				
Cubic $Fm\bar{3}m$	$a=0.5118$ nm	Zr	4a	
		O	8c	
Tetragonal $P4_2/nmc$	$a=0.3622$ nm, $c=0.5284$ nm	Zr	2a	
		O	4d	$z=0.05725$
Monoclinic $P2_1/c$	$a=0.5190$ nm, $b=0.5243$ nm,	Zr	4e	$x=0.2758$, $y=0.04372$, $z=0.2100$
	$c=0.5379$ nm, $\beta=99.65°$	O(1)	4e	$x=0.06513$, $y=0.3266$, $z=0.3498$
		O(2)	4e	$x=0.4509$, $y=0.7568$, $z=0.4755$
Orthorhombic $Pbca$	$a=1.015$ nm, $b=0.5299$ nm,	Zr	8c	$x=0.8843$, $y=0.03489$, $z=0.2519$
	$c=0.5132$ nm	O(1)	8c	$x=0.7888$, $y=0.3728$, $z=0.1247$
		O(2)	8c	$x=-0.02193$, $y=0.7388$, $z=0.4977$
Orthorhombic $Pnma$	$a=0.5599$ nm, $b=0.3375$ nm,	Zr	4c	$x=0.2490$, $z=0.1071$
	$c=0.6549$ nm	O(1)	4c	$x=-0.02120$, $z=0.6586$
		O(2)	4c	$x=0.3610$, $z=0.4223$
LDA (15 Ha)				
Cubic $Fm\bar{3}m$	$a=0.5028$ nm	Zr	4a	
		O	8c	
Tetragonal $P4_2/nmc$	$a=0.3558$ nm, $c=0.5110$ nm	Zr	2a	
		O	4d	$z=0.04260$
Monoclinic $P2_1/c$	$a=0.5085$ nm, $b=0.5183$ nm,	Zr	4e	$x=0.2777$, $y=0.04226$, $z=0.2094$
	$c=0.5240$ nm, $\beta=99.46°$	O(1)	4e	$x=0.07296$, $y=0.3420$, $z=0.3365$
		O(2)	4e	$x=0.4476$, $y=0.7582$, $z=0.4816$
Orthorhombic $Pbca$	$a=0.9973$ nm, $b=0.5212$ nm,	Zr	8c	$x=0.8848$, $y=0.03465$, $z=0.2531$
	$c=0.5030$ nm	O(1)	8c	$x=0.7907$, $y=0.3759$, $z=0.1292$
		O(2)	8c	$x=-0.02287$, $y=0.7389$, $z=0.4976$
Orthorhombic $Pnma$	$a=0.5521$ nm, $b=0.3283$ nm,	Zr	4c	$x=0.2454$, $z=0.1134$
	$c=0.6425$ nm	O(1)	4c	$x=-0.02587$, $z=0.6624$
		O(2)	4c	$x=0.3594$, $z=0.4268$

peratures T_j is then calculated as indicated in the next paragraph, and finally the $F(V_i,T_j)$ are interpolated at fixed T_j through an equation of state (EOS). The third-order Birch-Murnaghan (BM) EOS (Refs. 55 and 56) is used in the following. This procedure enables to find not only the evolution with temperature of the equilibrium free energy and volume at $p=0$ but also of the bulk modulus $B=-V\partial p/\partial V$.

The quasiharmonic approximation is expected to be reasonably accurate up to approximately half the melting temperature ($T_{\text{melt}}=2983\pm15$ K for zirconia[57]). Beyond this threshold, anharmonic effects (such as phonon-phonon interactions) become important; see Ref. 21 for a detailed discussion and application to cubic zirconia.

2. Free-energy computation

If N is the number of atoms in the primitive unit cell, and if we neglect (as zirconia is an insulator) the electronic contribution, the free energy F is the sum of the energy E_0 of the crystal at $T=0$ K (as computed by density-functional theory) and of the vibrational free-energy F_{vib} arising from the ionic motion

$$F = E_0 + F_{\text{vib}}, \tag{1}$$

the last term can be written

$$F_{\text{vib}} = 3N\int_0^{+\infty}\left[\frac{\hbar\omega}{2} + k_BT\ln(1-e^{-x})\right]g(\omega)d\omega,$$

where $x=\hbar\omega/k_BT$, $g(\omega)$ is the normalized density of states $[\int_0^{+\infty}g(\omega)d\omega=1]$, and k_B the Boltzmann constant. The internal energy $E=E_0+E_{\text{vib}}$ (including the zero-point energy), the entropy $S=-(\partial F/\partial T)_V$ and the heat capacity at constant volume $C_v=(\partial E/\partial T)_V$ can be computed as follows:

$$E_{\text{vib}} = 3N \int_0^{+\infty} \left[\frac{\hbar\omega}{2} + \frac{\hbar\omega}{e^x - 1} \right] g(\omega) d\omega,$$

$$S = 3Nk_B \int_0^{+\infty} \left[\frac{xe^x}{e^x - 1} - \ln(e^x - 1) \right] g(\omega) d\omega,$$

$$C_v = 3Nk_B \int_0^{+\infty} e^x \left[\frac{x}{e^x - 1} \right]^2 g(\omega) d\omega.$$

The molar values are deduced by multiplying these quantities by $\mathcal{N}_A \times 3/N$, $\mathcal{N}_A$ being the Avogadro constant, as there are $3\mathcal{N}_A$ atoms for each mole of ZrO_2. Finally, the heat capacity at constant pressure is given by $C_p = C_v + \alpha^2 V B_0 T$, where α the coefficient of thermal expansion at constant pressure $(\partial \ln V/\partial T)_p$.

3. Grüneisen parameters

The Grüneisen mode parameters γ_i (see, for instance, Refs. 50 and 51) are a measure of the volume dependence of the vibrational energy

$$\gamma_i = -\left(\frac{\partial \ln \nu_i}{\partial \ln V} \right)_{T,0} = -\frac{V_0}{\nu_{i,0}} \left(\frac{\partial \nu_i}{\partial V} \right)_{T,0},$$

where ν_i is the frequency (wave numbers) of the ith mode and the subscript 0 refers to the reference state at $p=0$. Grüneisen parameters lie generally between 1 and 2 (see Ref. 50). They are related to the variation in wave numbers with pressure by

$$\gamma_i = -\frac{V_0}{\nu_{i,0}} \left(\frac{\partial p}{\partial V} \right)_0 \left(\frac{\partial \nu_i}{\partial p} \right)_0 = \frac{B_0}{\nu_{i,0}} \left(\frac{\partial \nu_i}{\partial p} \right)_0. \quad (2)$$

III. STRUCTURAL PROPERTIES

A. Results at $p=0$, $T=0$

A summary of the structural properties of the five polymorphs, obtained for both GGA and LDA sets of potentials, is given in Table I; a full report including the elastic properties and further details regarding the GGA set are available in Ref. 23. Both the structural parameters obtained with the GGA set in Ref. 23 and those obtained with the LDA set in the present work are in line with the corresponding previously published computations.[23]

The ground-state energy of each phase at $p=0$ is given in Table II; the hierarchy is the same for both sets of potentials. As in a previous study,[42] the LDA gives energy differences systematically smaller than the GGA. An important consequence is the underestimate of the pressures and temperatures of transitions, as discussed in Secs. III C and V A, respectively.

B. Pressure dependence of the structural parameters

The variation with pressure of the lattice parameters is presented in Fig. 1 for the LDA; the GGA results are similar with, however, a larger dependence on pressure. Table III presents the compressibilities for the various polymorphs of zirconia. As expected, the LDA lowers the values of the compressibilities (compare with the GGA results given in Table III of Ref. 23).

TABLE II. Computed ground-state energy difference and bulk moduli, both at 0 K and $p=0$, of the various phases of zirconia. The relative difference ΔE is given with respect to the monoclinic polymorph for both LDA and GGA sets of potentials. The bulk modulus B_0 is obtained with the BM EOS in the LDA case. See Ref. 23 for other data on elastic properties.

	ΔE (meV/atom)		B_0 (GPa)	
Phase	LDA	GGA	LDA	GGA[a]
Monoclinic $P2_1/c$	0	0	165.6 ± 0.9	193
Orthorhombic $Pbca$	8.708	22.49	224.7 ± 0.5	210
Tetragonal $P4_2/nmc$	16.62	37.34	202.1 ± 0.2	172
Cubic $Fm\bar{3}m$	31.26	71.74	261.6 ± 0.2	235
Orthorhombic $Pnma$	41.34	114.6	262.8 ± 0.5	213

[a]Reference 23.

C. Enthalpy and pressures of transition

The thermodynamic potential at $T=0$ K is the enthalpy $H=E+pV$, where E is the internal energy, i.e., the E_0 of Eq. (1), p the pressure, and V the volume. Figure 2 represents, for the five polymorphs, the pressure dependence of the excess of enthalpy with respect to that of the monoclinic phase.

As can be seen, the orthorhombic $Pbca$ becomes the most favored phase at around 8 GPa (left arrow in Fig. 2; the computation with the interpolated BM EOS gives 7.97 GPa) but the orthorhombic $Pnma$ phase, in turn, becomes more energetically favored at 13.0 GPa (right arrow). As discussed above, LDA computations strongly underestimate these values, giving, respectively, 3.49 ± 0.01 GPa and 4.46 ± 0.02 GPa. The values obtained through the GGA are instead rather good. Indeed, the experimental data for the monoclinic-to-orthorhombic $Pbca$ transition vary between 3–4 (Refs. 17 and 59) and 10 GPa;[13,16] the present computation is within the experimental range and compares favorably with the transition pressure of 6.64 GPa computed through the GGA in Ref. 38.

The pressure experimentally observed for the orthorhombic $Pbca$ to orthorhombic $Pnma$ phase transition varies from 12.5 (Ref. 17) to 25 GPa (Refs. 13 and 16); Refs. 38 and 39 report 9.20 GPa and 19.1 GPa, respectively. Again the present computation is within the experimental range. This transition is characterized by an increase (from 7 to 9) in the Zr coordination number, typical of high-pressure packing (see, for instance, Refs. 60–62 and references therein).

It is interesting to note that, above 24 GPa, the monoclinic phase is computed to have the highest enthalpy of all phases, in total contrast with the situation at 0 GPa.

IV. PHONON SPECTRA

The conventional reciprocal cell and the notations of Miller and Love[63,64] for the high-symmetry points of the BZ

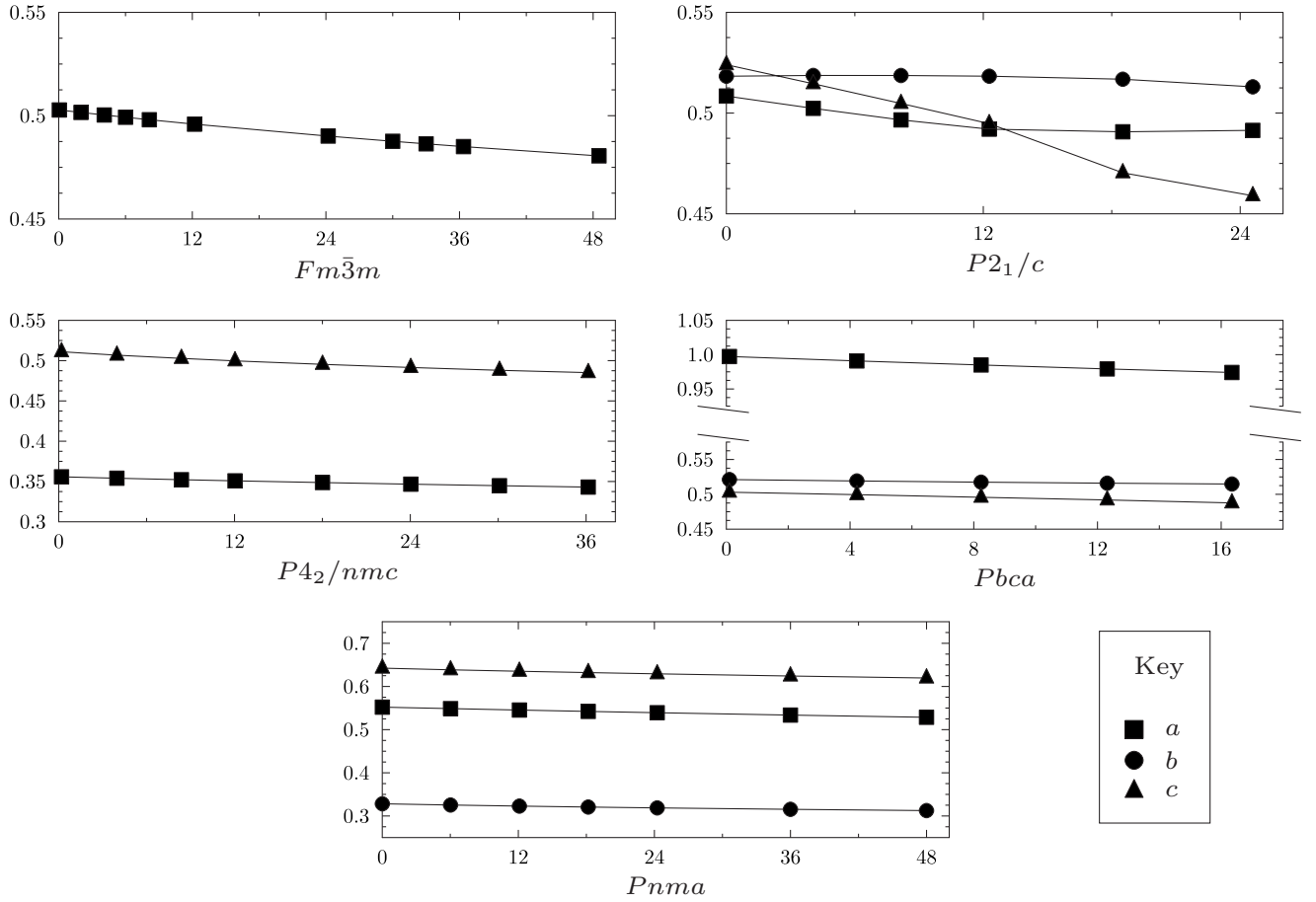

FIG. 1. Pressure dependence of lattice parameters for the five polymorphs of zirconia, as computed with the LDA set of pseudopotentials. Lattice parameters (a: filled squares, b: filled circles, and c: filled triangles) are in nm, pressure in GPa. The phase is indicated just below each panel. Lines joining the computed points are a guide for the eyes, not interpolations.

and the irreducible representations are used in the following. Wave vectors are given in reduced coordinates, i.e., in units of 2π over the lattice parameter of the given direction. There is a direct group-subgroup relationship between the symmetry groups of the cubic, tetragonal, and monoclinic phases;[65–67] but there exists no such relationship between the symmetry groups of the cubic and the two orthorhombic phases compatible with the number of atoms in the primitive cells and the respective Wyckoff positions, and none also between the two orthorhombic phases.

In the following we present the phonon-dispersion curves and density of states at $p=0$ and discuss their dependence on pressure.

A. Cubic $Fm\bar{3}m$ phase

It has been observed experimentally that the cubic phase is not stable until 2650 K (see, for instance, Refs. 3, 13, and 68). From a group-theoretical analysis,[65] in this case symmetry allows for an instability related to the X_2^- irreducible representation of $Fm\bar{3}m$, whose eigenmode has atomic displacements of the oxygen sublattice along the cubic fourfold axes, leading to the tetragonal polymorph (see Fig. 3 in Ref. 65); this X-point instability is confirmed by several computations[6,18,20,21,69] (at $T=0$, except for Ref. 21).

Figure 3 represents the phonon-dispersion curves for the GGA (dashed) and LDA potentials (continuous lines). As

TABLE III. Compressibilities (in 10^{-3} GPa^{-1}) of the zirconia phases, as computed with the LDA set of pseudopotentials.

Phase	$\chi_{[100]}$	$\chi_{[010]}$	$\chi_{[001]}$
$Fm\bar{3}m$		0.9266 ± 0.0218	
$P4_2/nmc$		0.9847 ± 0.0293	1.393 ± 0.071
$P2_1/c$	1.365 ± 0.350	0.3900 ± 0.1255	5.264 ± 0.2688
$Pbca$	1.439 ± 0.031	0.7547 ± 0.0421	1.877 ± 0.041
$Pnma$	0.8869 ± 0.0207	0.9874 ± 0.0553	0.7339 ± 0.0296

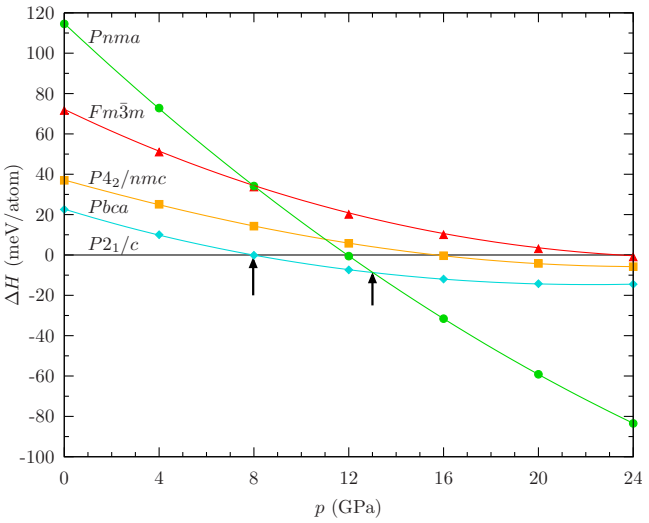

FIG. 2. (Color online) Relative enthalpy at 0 K $\Delta H(p)=H(p)-H_m(p)$ of the various phases of zirconia with respect to the enthalpy of the monoclinic phase at the given pressure p. The space group of each phase is indicated above each curve (obtained from the interpolated BM EOS); symbols refer to computations (GGA set). The two arrows indicate the transition pressures, see text.

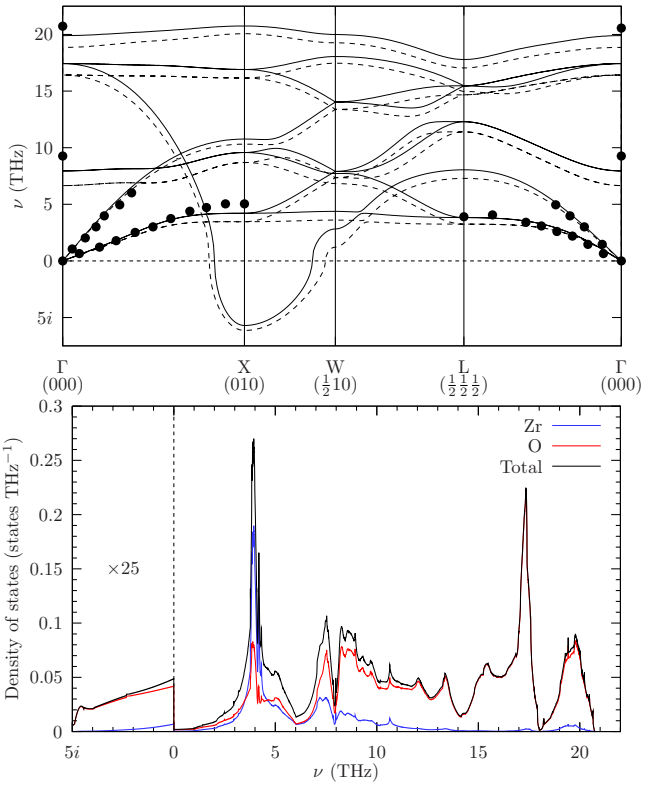

FIG. 3. (Color online) Phonon-dispersion curve (top) and density of states (bottom) at $p=0$ of the cubic phase (LDA only for the latter). In the top panel, continuous/dashed lines refer to LDA/GGA computations, respectively, and the filled circles to neutron-scattering data (Ref. 70). The imaginary part of the density of states (left of the dashed vertical line) is magnified by a factor of 25 for clarity.

expected, two main features appear: (i) to the X point and more precisely to the X_2^- eigenmode, corresponds an instability; (ii) the GGA values of the phonon frequencies are systematically lower than their LDA counterparts.

The computed acoustic branches are in good agreement with the neutron scattering data[70] on a stabilized sample (Y_2O_3 at 20 mol %); there is, however, disagreement on the infrared optical measurements (filled circles on the Γ line at around 10 and 20 THz), see the end of this section for the LDA values of the frequencies. The discrepancy is caused by doping; indeed, for a high concentration of dopants, structural disorder associated with oxygen vacancies[71] (as Y is trivalent whereas Zr is tetravalent) has noticeable effects on the infrared and Raman spectra.[72–75] The flattening of the lowest acoustic branch at the W point is also observed at higher cutoff energies and BZ sampling, and (even if not as clearly) in Ref. 20, Fig. 1.

As remarked in the latter work, the zirconium ions, being about six times heavier than the oxygen ions, contribute almost only to the low-frequency (less than 10 THz) modes. In all polymorphs the oxygen ions are responsible instead of the high-frequency modes; in the cubic case, the latter are also responsible for the unstable modes.[65] The eigenmodes of all phases are generally mixed bending-stretching modes, which might be seen as more or less distorted and asymmetric "breathing" modes of the Zr coordination polyhedron. The density of states is characterized by two strong peaks: the first one corresponds to the X-W-L part of the stable acoustic branches (see Fig. 3), whereas the second one corresponds to the frequency domain of the Raman-active T_{2g} mode (see Table IV in Part II).

As pressure increases, the square of the frequency at the X point increases until becoming positive between 30 and 33 GPa; Ref. 21 found the same behavior when increasing temperature. The Grüneisen parameters at the Γ point are all positive; the values for the infrared-active T_{1u} mode at 7.95 THz (265.1 cm^{-1}, TO) and 19.90 THz (663.9 cm^{-1}, LO) are 4.138 ± 0.007 and 1.186 ± 0.016, respectively. We have found 1.499 ± 0.020 for the T_{2g} Raman-active mode at 17.43 THz (581.4 cm^{-1}); the first value is unusually high and the discussion in the next paragraph on the tetragonal E_u modes applies also here.

B. Tetragonal $P4_2/nmc$ phase

The tetragonal phase is known experimentally to be stable above 1400 K; owing to the wide field of applications of the tetragonal-to-monoclinic transition in ceramics toughening, the respective domain of stability of the two phases has been studied extensively (see, for instance, Refs. 3, 44, 68, and 76–80); yet a detailed microscopic mechanism for the transition, on which all authors agree, appears to be still lacking. A group-theoretical investigation[66] shows that the simultaneous activation of two modes [corresponding to the irreducible representations M_1 and M_2 of the $M=(\frac{1}{2}\frac{1}{2}0)$ point] gives a possible mechanism; see Fig. 3 in Ref. 66. A related mechanism has been described in Ref. 9; both works agree with many experiments on the relative crystallographic orientation of the monoclinic and tetragonal phases. On the other hand, a different mechanism, related to the activation

TABLE IV. Grüneisen mode parameters at the Γ point for the tetragonal phase; indicated wave numbers (in cm^{-1}) are at $p=0$. The parameters have been computed by linear interpolation for pressures between −12 and 12 GPa corresponding to the linear regime. The pressure dependence of the frequencies is computed using Eq. (2) and the value of the bulk modulus at 0 K found in Table II.

Infrared		ν_i (cm^{-1})	γ_i
A_{2u}	(TO)	333.5	0.883 ± 0.013
	(LO)	653.7	1.06 ± 0.03
E_u	(TO)	148.3	8.91 ± 0.29
	(LO)	261.9	0.479 ± 0.042
E_u	(TO)	440.1	3.72 ± 0.19
	(LO)	725.8	0.221 ± 0.009

Raman	ν_i (cm^{-1})	γ_i	$(\partial\nu/\partial p)_0$ (cm^{-1} GPa^{-1}) LDA[a]	LDA[b]	Expt.[c]
A_{1g}	264.8	-2.52 ± 0.28	-3.30 ± 0.37	−3.77	−3.59
B_{1g}	323.2	2.35 ± 0.03	3.76 ± 0.04	3.03	3.43
	598.3	0.886 ± 0.032	2.62 ± 0.10	2.53	2.41
E_g	144.5	2.69 ± 0.04	1.92 ± 0.03	1.49	1.75
	464.6	2.25 ± 0.14	5.17 ± 0.32	5.14	5.58
	647.0	0.829 ± 0.011	2.65 ± 0.04	2.30	2.79

Silent	ν_i (cm^{-1})	γ_i
B_{2u}	661.8	1.40 ± 0.03

[a]Present computation.
[b]Reference 22.
[c]Reference 83.

of a *Z*-point instability, agrees with some other experimental data on the orientation relationships, see Ref. 81 and references therein.

First-principles computations have so far not been able to help clarify this issue, as no instabilities have been observed at 0 K; the distance to the transition temperature (which is between 1200 and 1500 K, see Ref. 44) might explain this. In Ref. 82, the authors found the *M* unstable mode by using a lattice-dynamical treatment and by computing the phonon spectrum in the neighborhood of the transition temperature (1400 K). In Fig. 4 we also notice the low value of the smallest frequency at the *Z* point, lower than that at the *M* point, in agreement with Ref. 20.

The density of states bears many similarities with its cubic equivalent but also shows the dense occupation of states (because of an increased number of atoms in the primitive cell) which is typical of the monoclinic and the two orthorhombic polymorphs from 2.5 to 18 THz, as well as a gap around 19.5 THz and a strong peak near 20.75 THz, a feature also found in the orthorhombic *Pnma* phase.

Table IV summarizes the LDA results for the Grüneisen parameters of the optical modes. The GGA results show again a strong systematic softening (as seen in Fig. 4) averaging 4.5% (root mean square of the relative errors) and (by overestimate of the equilibrium volume) a marked difference with the LDA results as to the pressure dependence. This is further amplified for the two E_u infrared-active modes, which exhibit high values of the Grüneisen parameters and are thus very sensitive to volume changes. This explains (see Part II) the failure of the GGA potentials to correctly estimate the dielectric permittivity tensor. The LDA results are on the other hand quite satisfactory and show a good agreement with experimental Raman spectroscopy data[83] (see Table IV).

Another interesting point is the existence of a negative value of the Grüneisen parameter for the A_{1g} Raman-active mode, which should lead to a Γ-point loss of stability of the tetragonal phase as pressure increases. Reference 22 shows, however, that a transition to the cubic phase occurs at 37 GPa, before the loss of stability of the A_{1g} mode; we have indeed checked with a direct computation at 36 GPa that (i) the wave number for the A_{1g} mode is still positive (52.0 cm^{-1}) but the Raman activity of this mode has practically vanished (see Fig. 2 in Part II); (ii) the c/a ratio is nearly $\sqrt{2}$ and the atoms are almost in the positions they occupy in the cubic phase, and (iii) the anisotropy factor of the static dielectric tensor $\epsilon_{33}/\epsilon_{11}$ is 0.979, very close to 1.

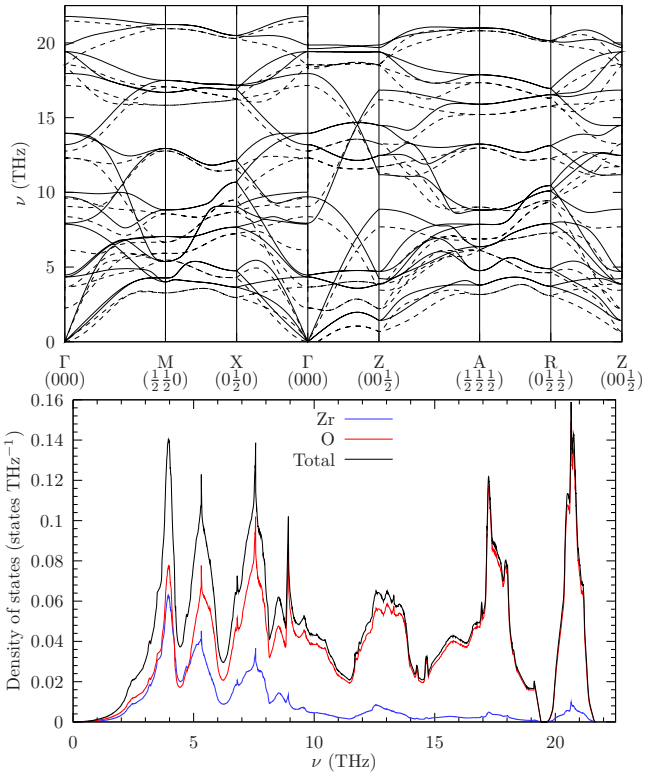

FIG. 4. (Color online) Phonon-dispersion curve along the high-symmetry directions of the BZ (top) and density of states (bottom) at $p=0$ of the tetragonal phase (LDA only for the latter). Continuous/dashed lines in the top panel refer to LDA/GGA computations, respectively. No soft modes are observed.

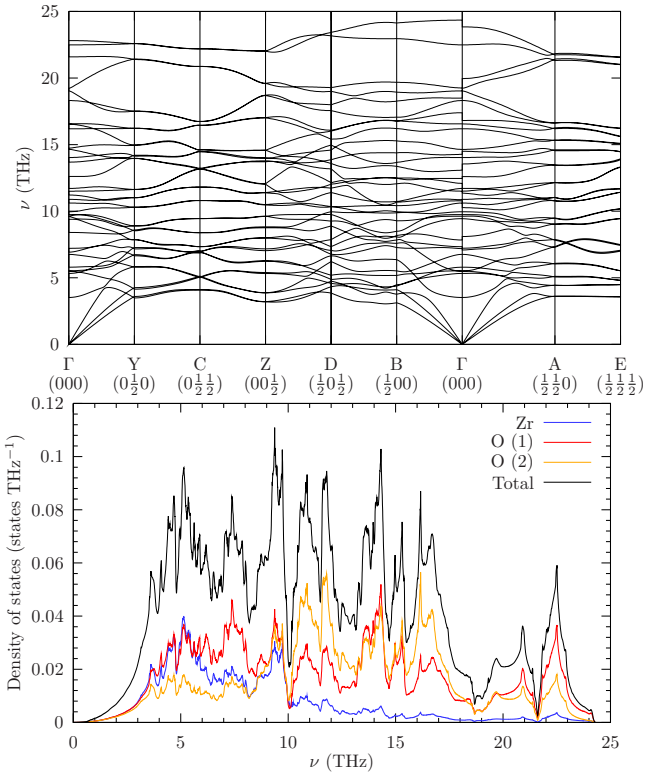

FIG. 5. (Color online) Phonon-dispersion curve along the high-symmetry directions of the BZ (top) and density of states (bottom) at $p=0$ of the monoclinic phase (LDA). No soft modes are observed.

C. Monoclinic $P2_1/c$ phase

The monoclinic phase is the only naturally observed polymorph (as the rare mineral baddeleyite); it is therefore believed to be globally stable at ambient conditions. Monoclinic zirconia is indeed computed to be the most stable polymorph at ambient pressure by all references[23,29,38,42,84,85] except Ref. 39.

Present computations of the phonon spectrum at $p=0$, as seen in Fig. 5, show no signs of instability and no particular features. Given the larger number of atoms in the primitive cell, the density of states looks more like a broadband with some less-prominent peaks; a distinctive feature, found also with the two orthorhombic polymorphs, is the strong and relatively constant contribution of Zr ions up to 10 THz.

The monoclinic phase has several modes with negative Grüneisen parameters, most notably some infrared-active (A_u at 183.8 and 239.7 cm^{-1}, B_u at 230.7 cm^{-1}), and some Raman-active modes (B_g at 320.7 and 488.2 cm^{-1}); the values are, however, not always numerically well constrained. The maximal value is obtained for the LDA case at 2.70 ± 0.23 (A_g at 193.2 cm^{-1}); the GGA gives instead 3.74 ± 0.64 for the same mode with a wave number of 98.8 cm^{-1}. A direct computation with the LDA potentials at 24 GPa shows the existence of an unstable branch along the D-B line with a minimum close to the B point; this behavior is neither observed at lower pressures nor confirmed by the GGA computations. Such instability cannot be related to the transition to the orthorhombic *Pbca* polymorph, known experimentally to occur between 3–4 (Refs. 17 and 59) and 10 GPa (Refs. 13 and 16), see Sec. III C above.

D. Orthorhombic *Pbca* phase

The *Pbca* polymorph has the lowest enthalpy at zero pressure of all phases except the monoclinic;[23,38,84] it has, however, not been recovered at ambient conditions (see Fig. 3 of Ref. 81 and Ref. 59). The *Pbca* structure is somewhat anomalous for a high-pressure phase, having a rather low coordination number (7, against 8 for the cubic and tetragonal polymorphs) and a relatively open structure; for instance, its calculated mass density is almost equal to that of the tetragonal phase and smaller than that of the cubic phase (5900 for both $P4_2/nmc$ and *Pbca* against 6100 kg m^{-3} for $Fm\bar{3}m$ polymorphs), and its packing ratio is 0.40 just as the tetragonal phase, against $3\pi\sqrt{3}/32 \approx 0.51$ for the fluorite structure.

The dispersion curve, depicted in Fig. 6, does not show any particular features; no gaps are noticeable with the exception of the 15 THz region. The density of states shows instead strong coupling among the three orbits in the crystal below 10 THz, just as in the monoclinic case, but also between the two oxygen orbits above 10 THz. This indicates that, for the high-frequency bending modes, all Zr-O bonds are nearly equivalent (in spite of the separation of oxygen ions into two crystallographic orbits).

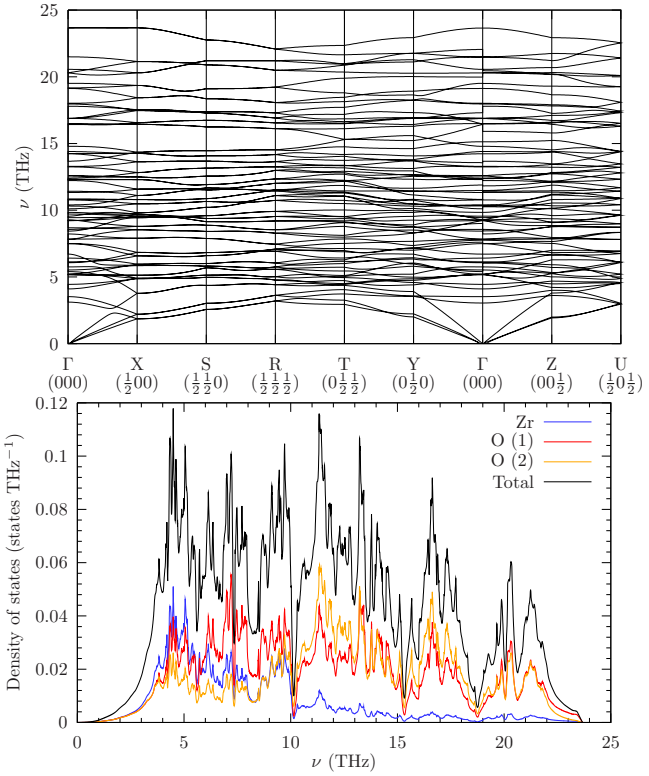

FIG. 6. (Color online) Phonon-dispersion curve along the high-symmetry directions of the BZ (top) and density of states (bottom) at $p=0$ of the orthorhombic *Pbca* phase. No soft modes are observed.

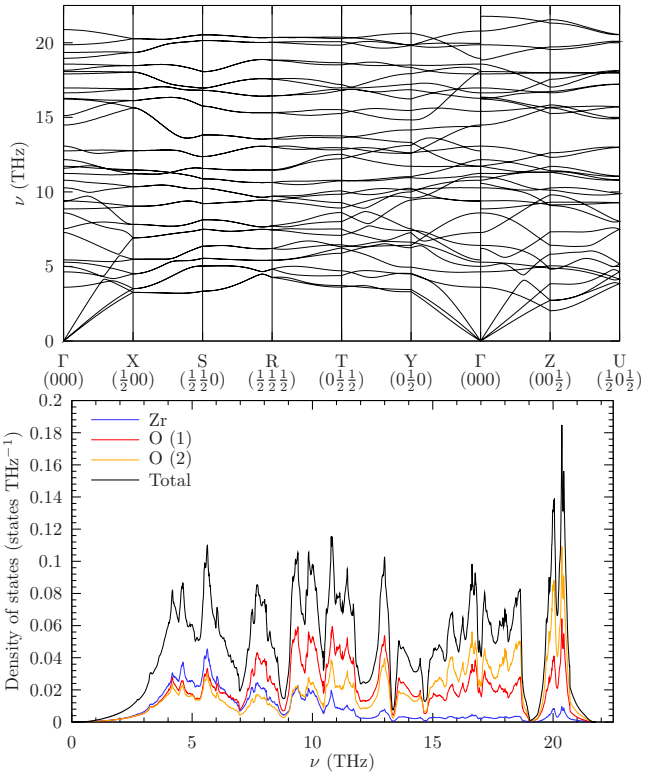

FIG. 7. (Color online) Phonon-dispersion curve along the high-symmetry directions of the BZ (top) and density of states (bottom) at $p=0$ of the orthorhombic *Pnma* phase. No soft modes are observed.

The Grüneisen parameters at the Γ point are all positive, ranging from 0.277 ± 0.06 (B_{1u} at 180.2 cm^{-1}) to 2.82 ± 0.04 (B_{1u} at 410.4 cm^{-1}); both modes are infrared active. No negative parameters have been found elsewhere in the BZ (just as for the cubic case). The transitions to either the tetragonal[3,59] or the *Pnma* phase (discussed in Sec. III C above) are therefore not expected to be driven by vibrational instabilities, see Refs. 59, 86, and 87 and references therein.

E. Orthorhombic *Pnma* phase

The second orthorhombic polymorph is the high-pressure form of zirconia.[15,23,38,42] However, in contrast to the *Pbca* polymorph, the *Pnma* phase has been recovered at ambient pressure;[15] it is therefore expected not to exhibit soft modes at $p=0$ GPa. This phase is characterized by the highest coordination number (9) among all zirconia phases for Zr ions and also the highest mass density (6600 against 5700 $kg\ m^{-3}$ for the monoclinic polymorph), typical of high-pressure structural modifications; it is, however, still an open structure, having a packing ratio of 0.506 at zero pressure, implying a strong rigidity of the Zr-O bonds.

The dispersion curve, Fig. 7, shows no particular features, just as for the monoclinic and the orthorhomic *Pbca* phases. The density of states is very similar to that of the monoclinic phase with, however, a noticeable gap at 19 THz (similar to the one seen for the tetragonal phase) and a strong peak at 20 THz (bond bending).

At the Γ point, the Grüneisen parameters range from 0.983 ± 0.03 (Raman-active A_g mode at 435.7 cm^{-1}) to 4.37 ± 0.37 (infrared-active B_{1u} mode at 181.2 cm^{-1}). Exactly as for the other orthorhombic polymorph, the *Pnma* phase has no negative Grüneisen parameters in the whole BZ. This is consistent with the fact that no other high-pressure polymorph is known to exist; indeed, the observations of a new high-pressure phase[11,12] have not been confirmed by later experiments.

V. THERMOELASTIC PROPERTIES

A. Monoclinic-to-tetragonal phase transition

As discussed above, the monoclinic-to-tetragonal phase transition, which occurs between 1200 and 1500 K, is of great importance because of its relevance, for instance, in ceramics toughening (see Refs. 3 and 4 and references therein). A summary of the published literature regarding the thermodynamic data on the transition is available in a recent paper;[44] see also the references in Ref. 81.

The LDA computations predict (see Table V) a transition temperature of about 960 K, which is too low;[44] this is a consequence of the underestimate of the ground-state energy difference between the tetragonal and monoclinic phases. The GGA gives a much better result, see again Table V; computed calorimetric properties in the GGA case are in line with the experimental results published in Ref. 44. The relative change in volume is $1-V_t/V_m=3.5\%$, comparable to the

TABLE V. Computed parameters of the monoclinic-to-tetragonal phase transition.

Potentials	T (K)	ΔS (J K^{-1} mol^{-1})	$\Delta H=T\Delta S$ (kJ mol^{-1})
LDA	970 ± 5	2.964	2.875
GGA	1345 ± 5	4.862	6.552

experimental value of 3.2% at 1480 K reported in Ref. 78.

B. Thermal expansion

We present the results first in the tetragonal and monoclinic cases for which experimental data are available (see Fig. 8). The agreement with experiment is very good in the monoclinic case for both the LDA and GGA results. This is also true for the tetragonal case, which, however, offers a typical example of the experimental difficulties faced with zirconia: "[…] it is not clear with which of the different experimental data the theory must agree."[25] Indeed, in this case the LDA shows a good agreement with Ref. 88 (neutron-diffraction data), even though it underestimates the high-temperature (>2000 K) expansion, as a consequence

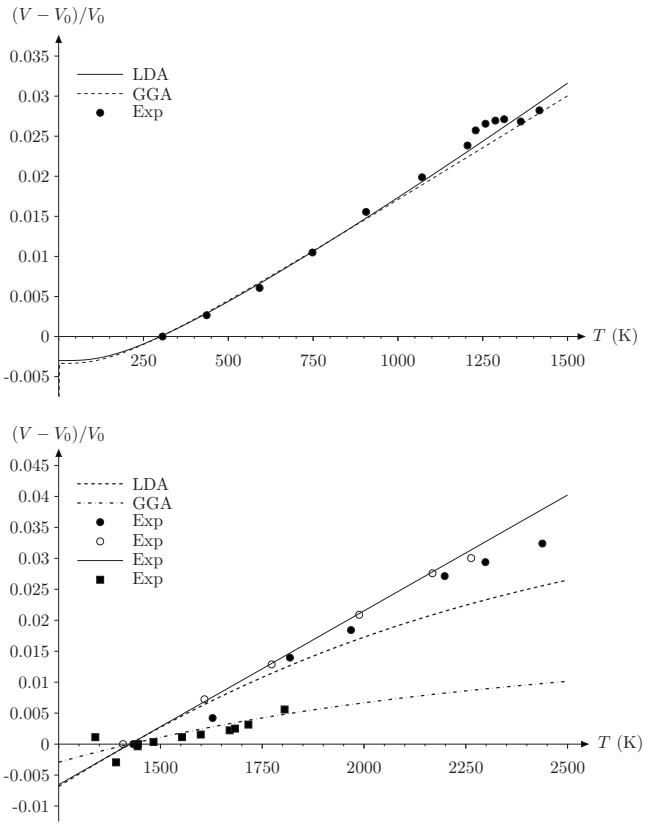

FIG. 8. (Top) Relative volume variation for the monoclinic phase; filled circles are experimental data (Ref. 89). (Bottom) Relative volume variation for the tetragonal phase. Circles (filled: neutral atmosphere, empty: reducing atmosphere) correspond to Ref. 88, the continuous straight line to the interpolation given by the author of Ref. 90 and the filled squares to Ref. 78.

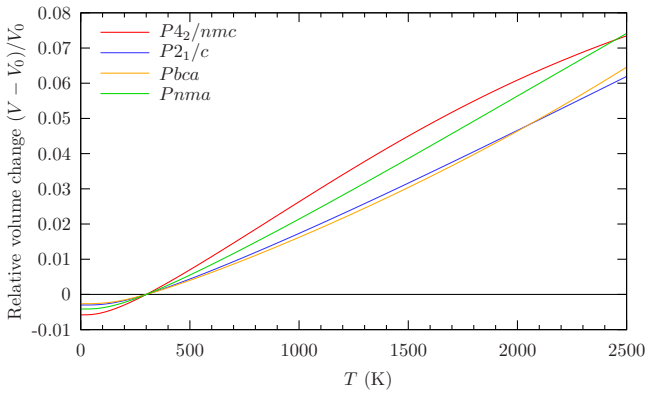

FIG. 9. (Color online) Computed relative volume variation in four polymorphs of zirconia (LDA); the reference temperature is 300 K.

of the limited validity at high temperatures of the quasiharmonic approximation presently used. On the contrary, the GGA results are in poor agreement with these data, but in very good agreement with those in Ref. 78 (also neutron diffraction). Twinning in the monoclinic samples[13] might be the cause for the experimental discrepancies.

The thermal expansion of all polymorphs but the cubic phase (see Sec. II A 3) is illustrated in Fig. 9; the relative volume change is very similar for all the four examined polymorphs.

C. Entropy and heat capacities

The results for the monoclinic phase only are given, as no other experimental data are available. As seen in Fig. 10, the agreement with experiment is very good in both the LDA and GGA cases.

D. Bulk modulus

We present the LDA results regarding the bulk modulus of the same four phases. Apart from the tetragonal phase, which exhibits an anomalous increase in the bulk modulus with temperature (which might be a consequence of the quasiharmonic approximation), the other phases show a decline. The computed behavior for the monoclinic polymorph is at variance with available experimental data,[93] both in magnitude and in trend (see Fig. 11), as the computations of Ref. 29; it should, however, be noted that the value of the compressibility $\chi_{[010]}$ as deduced from Ref. 93 is negative, which implies that these experimental data are not completely reliable.

VI. CONCLUSIONS

The phonon spectra and densities of states of the five known zirconia polymorphs have been computed through density-functional perturbation theory to a pressure of 48 GPa. The agreement with the available published data is generally good, both computational and experimental. We find that these properties in the two high-pressure orthorhombic phases are similar to those in the monoclinic polymorph, as was already observed for the elastic moduli in a previous

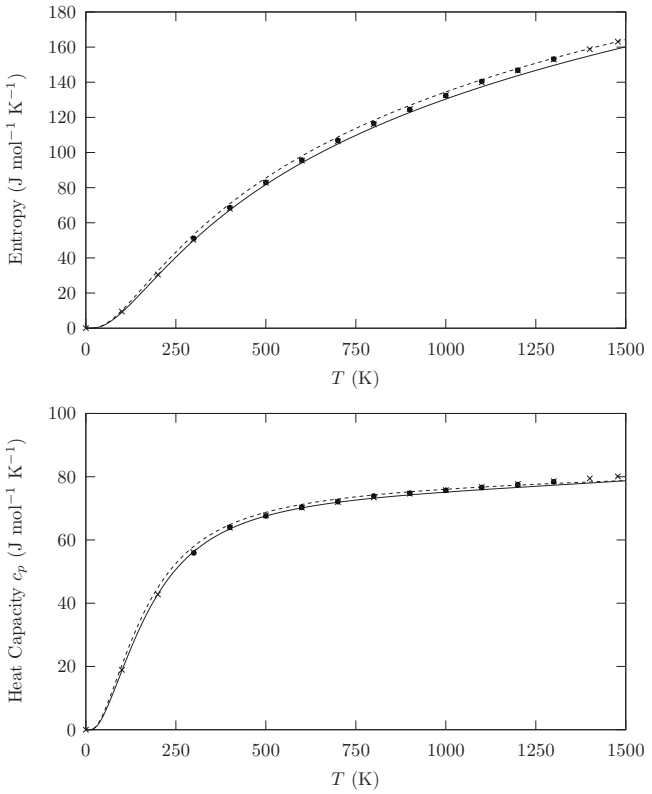

FIG. 10. Entropy (top) and heat capacity at constant pressure (bottom) as a function of temperature for monoclinic zirconia; filled circles (Ref. 91) and crosses (Ref. 92) are experimental data; solid (LDA) and dashed (GGA) lines represent the computations.

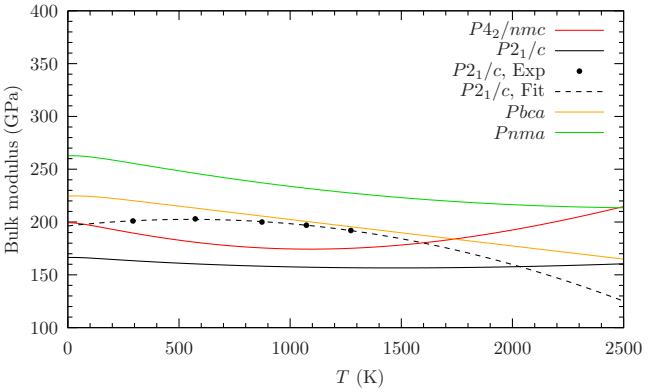

FIG. 11. (Color online) Bulk modulus of four phases of zirconia as a function of temperature; the dashed line is an interpolation of the experimental data (filled circles, Ref. 93).

investigation.[23] As for hafnia,[28] the GGA leads to a systematic phonon softening with respect to the LDA; this comes from the large positive values of the Grüneisen mode parameters.

Within the quasiharmonic approximation, several thermoelastic quantities have been computed, as they are interesting *per se* and also constitute an indirect check on the phonon computations. We find the thermoelastic experimental data to be in very good agreement with either the GGA or the LDA results (see especially thermal expansion in Fig. 8), depending on the selected experimental data; for the GGA we also obtain rather good values of the transition pressures (Fig. 2). The LDA, on the other hand, is fairly good overall, giving good results for the dielectric constants (Part II), but transition pressures and temperatures in poor agreement with experiment.

Cubic zirconia is computed to be unstable up to 2570 K (Ref. 21) and 31.5 ± 1.5 GPa (present computations) because of a soft mode at the X point. We have confirmed the existence of a stability exchange between the tetragonal and cubic phases at around 36 GPa, as previously indicated in Refs. 22 and 83. However, at 0 K, the enthalpy of the cubic phase remains higher than that of the orthorhombic *Pnma* phase, even beyond 48 GPa (see Fig. 2); for instance, $\Delta H = 196$ meV/atom at 36 GPa and 227 meV/atom at 48 GPa (LDA); therefore the *Pnma* polymorph remains the observed structure in that range of pressures.

The monoclinic and tetragonal phases both experience a phonon-softening instability. For the first, this is computed to occur between 18 and 24 GPa according to our LDA calculations. For the second, the tetragonal phase is known to undergo a transition to the monoclinic phase around 1200–1500 K (see Ref. 44 and references therein); two possible mechanisms based on different orientation relationships have been proposed in Refs. 66 and 94. While the method of Ref. 21 is computationally expensive, it may, in principle, help clarify the transition mechanism at high temperatures, given that, in both our computations and in Ref. 20, the smallest frequency at 0 K at the Z point has a lower value than that at the M point.

The two orthorhombic phases have been computed to exhibit no vibrational instabilities; this is expected at least for the *Pnma* polymorph, as no other high-pressure phases are known and suggests other mechanisms than phonon softening for the *Pbca*-to-*Pnma* transformation. This goes along with the fact that, given the very different structures (see Fig. 1 of Ref. 23) of these two polymorphs, large atomic displacements are involved in this phase transition, in order to increase the periodicity along $[100]_{Pbca}$ and the coordination number of Zr ions.

ACKNOWLEDGMENTS

We acknowledge the partial support of the MATHMAT and MATHXPRE Projects of the Università di Padova, Italy. The computations were done on the cluster of the Cybersar at the Università di Cagliari, Italy.

*fadda@dsf.unica.it
†zanzotto@dmsa.unipd.it
‡luciano.colombo@dsf.unica.it

[1] J.-P. Cuif, E. Rohart, P. Macaudière, C. Bauregard, E. Suda, B. Pacaud, N. Imanaka, T. Masui, and S. Tamura, in *Binary Rare Earth Oxides*, edited by G. Adachi, N. Imanaka, and Z. C. Kang (Kluwer Academic, New York, 2005), Chap. 9.
[2] A. Medevielle, F. Thévenot, and D. Tréheux, J. Eur. Ceram. Soc. **15**, 1193 (1995).
[3] *Zirconia Engineering Ceramics*, edited by E. H. Kisi (Trans Tech, Ütikon-Zürich, 1998).
[4] R. C. Garvie, R. J. H. Hannink, and R. T. Pascoe, Nature (London) **258**, 703 (1975).
[5] G. Stapper, M. Bernasconi, N. Nicoloso, and M. Parrinello, Phys. Rev. B **59**, 797 (1999).
[6] X. Zhao and D. Vanderbilt, Phys. Rev. B **65**, 075105 (2002).
[7] I. Clarke *et al.*, J. Bone Jt. Surg., Am. Vol. **85**, 73 (2003).
[8] L. Gremillard, J. Chevalier, T. Epicier, S. Deville, and G. Fantozzi, J. Eur. Ceram. Soc. **24**, 3483 (2004).
[9] D. Simeone, G. Baldinozzi, D. Gosset, M. Dutheil, A. Bulou, and T. Hansen, Phys. Rev. B **67**, 064111 (2003).
[10] T. Arima, S. Yamasaki, K. Yamahira, K. Idemitsu, Y. Inagaki, and C. Degueldre, J. Nucl. Mater. **352**, 309 (2006).
[11] H. Arashi, T. Yagi, S. Akimoto, and Y. Kudoh, Phys. Rev. B **41**, 4309 (1990).
[12] O. Ohtaka, T. Yamanaka, and T. Yagi, Phys. Rev. B **49**, 9295 (1994).
[13] J. M. Léger, P. E. Tomaszewski, A. Atouf, and A. S. Pereira, Phys. Rev. B **47**, 14075 (1993).
[14] J. Haines, J. M. Léger, and A. Atouf, J. Am. Ceram. Soc. **78**, 445 (1995).
[15] J. Haines, J. M. Léger, S. Hull, J. P. Petitet, A. S. Pereira, C. A. Perottoni, and J. A. H. da Jornada, J. Am. Ceram. Soc. **80**, 1910 (1997).
[16] S. Desgreniers and K. Lagarec, Phys. Rev. B **59**, 8467 (1999).
[17] O. Ohtaka, H. Fukui, K. Funakoshi, W. Utsumi, T. Irifune, and T. Kikegawa, High Press. Res. **22**, 221 (2002).
[18] K. Parlinski, Z. Q. Li, and Y. Kawazoe, Phys. Rev. Lett. **78**, 4063 (1997).
[19] G.-M. Rignanese, F. Detraux, X. Gonze, and A. Pasquarello, Phys. Rev. B **64**, 134301 (2001).
[20] M. Sternik and K. Parlinski, J. Chem. Phys. **122**, 064707 (2005).
[21] P. Souvatzis and S. P. Rudin, Phys. Rev. B **78**, 184304 (2008).
[22] V. Milman, A. Perlov, K. Refson, S. J. Clark, J. Gavartin, and B. Winkler, J. Phys.: Condens. Matter **21**, 485404 (2009).
[23] G. Fadda, L. Colombo, and G. Zanzotto, Phys. Rev. B **79**, 214102 (2009).
[24] M. A. Caravaca, J. C. Miño, V. J. Pérez, R. A. Casali, and C. A. Ponce, J. Phys.: Condens. Matter **21**, 015501 (2009).
[25] A. P. Mirgorodsky and P. E. Quintard, J. Am. Ceram. Soc. **82**, 3121 (1999).
[26] G. Fadda, G. Zanzotto, and L. Colombo, following paper, Phys. Rev. B **82**, 064106 (2010).
[27] F. Favot and A. Dal Corso, Phys. Rev. B **60**, 11427 (1999).
[28] X. Zhao and D. Vanderbilt, Phys. Rev. B **65**, 233106 (2002).
[29] A. Kuwabara, T. Tohei, T. Yamamoto, and I. Tanaka, Phys. Rev. B **71**, 064301 (2005).
[30] QUANTUM-ESPRESSO is a community project for high-quality quantum-simulation software based on density-functional theory and coordinated by P. Giannozzi. See http://www.quantum-espresso.org and http://www.pwscf.org
[31] D. Vanderbilt, Phys. Rev. B **41**, 7892 (1990).
[32] J. P. Perdew, K. Burke, and M. Ernzerhof, Phys. Rev. Lett. **77**, 3865 (1996).
[33] S. G. Louie, S. Froyen, and M. L. Cohen, Phys. Rev. B **26**, 1738 (1982).
[34] J. P. Perdew and A. Zunger, Phys. Rev. B **23**, 5048 (1981).
[35] D. M. Ceperley and B. J. Alder, Phys. Rev. Lett. **45**, 566 (1980).
[36] D. Vanderbilt, USPP, available at http://www.physics.rutgers.edu/~dhv/uspp/
[37] H. J. Monkhorst and J. D. Pack, Phys. Rev. B **13**, 5188 (1976).
[38] J. E. Jaffe, R. A. Bachorz, and M. Gutowski, Phys. Rev. B **72**, 144107 (2005).
[39] J. K. Dewhurst and J. E. Lowther, Phys. Rev. B **57**, 741 (1998).
[40] J. E. Lowther, J. K. Dewhurst, J. M. Léger, and J. Haines, Phys. Rev. B **60**, 14485 (1999).
[41] C.-Z. Fan, S.-Y. Zeng, L.-X. Li, Z.-J. Zhan, R.-P. Liu, W.-K. Wang, P. Zhang, and Y.-G. Yao, Phys. Rev. B **74**, 125118 (2006).
[42] G. Jomard, T. Petit, A. Pasturel, L. Magaud, G. Kresse, and J. Hafner, Phys. Rev. B **59**, 4044 (1999).
[43] A. Dal Corso and S. de Gironcoli, Phys. Rev. B **62**, 273 (2000).
[44] X. Luo, W. Zhou, S. V. Ushakov, A. Navrotsky, and A. A. Demkov, Phys. Rev. B **80**, 134119 (2009).
[45] S. Baroni, S. de Gironcoli, A. del Corso, and P. Gianozzi, Rev. Mod. Phys. **73**, 515 (2001).
[46] X. Gonze and C. Lee, Phys. Rev. B **55**, 10355 (1997).
[47] G. Lehmann and M. Taut, Phys. Status Solidi B **54**, 469 (1972).
[48] P. E. Blöchl, O. Jepsen, and O. K. Andersen, Phys. Rev. B **49**, 16223 (1994).
[49] N. W. Ashcroft and N. D. Mermin, *Solid-State Physics* (Saunders/Harcourt College, Fort Worth, Philadelphia, 1976).
[50] O. L. Anderson, *Equations of State of Solids for Geophysics and Ceramic Science*, Oxford Monographs on Geology and Geophysics Vol. 31 (Oxford University Press, New York, 1995).
[51] G. Grimvall, *Thermophysical Properties of Materials* (Elsevier, Amsterdam, 1999).
[52] J.-P. Poirier, *Introduction to the Physics of the Earth's Interior*, 2nd ed. (Cambridge University Press, Cambridge, 2000).
[53] Ch. Kittel, *Introduction to Solid State Physics*, 8th ed. (Wiley, New York, 2005).
[54] A. A. Maradudin, E. W. Montroll, G. H. Weiss, and I. P. Ipatova, *Theory of Lattice Dynamics in the Harmonic Approximation*, 2nd ed. (Academic Press, New York, 1971).
[55] F. D. Murnaghan, Am. J. Math. **49**, 235 (1937).
[56] F. Birch, Phys. Rev. **71**, 809 (1947).
[57] R. J. Ackermann, S. P. Garg, and E. G. Rauh, J. Am. Ceram. Soc. **60**, 341 (1977).
[58] *International Tables for Crystallography, Volume A: Space-group symmetry*, edited by Th. Hahn (Springer, for the International Union of Crystallography, Dordrecht, 2006).
[59] S. Block, J. A. H. da Jornada, and G. J. Piermarini, J. Am. Ceram. Soc. **68**, 497 (1985).
[60] *Phase Transformations in Materials*, edited by G. Kostorz (Wiley-VCH, Weinheim, New York, 2001).
[61] *High-Pressure Geochemistry and Mineral Physics*, Developments in Geochemistry Vol. 9, edited by S. Mitra (Elsevier, Amsterdam, 2004).
[62] E. Y. Tonkov and E. G. Ponyatovsky, *Phase Transformations of Elements under High Pressure* (CRC Press, Boca Raton, 2005).
[63] S. C. Miller and W. F. Love, *Tables of Irreducible Representa-*

tions of Space Groups and Co-Representations of Magnetic Space Groups (Pruett Press, Boulder, Colorado, 1967).
[64] A. P. Cracknell, B. L. Davies, S. C. Miller, and W. F. Love, *General Introduction and Tables of Irreducible Representations of Space Groups*, Kronecker Product Tables, Vol. 1 (IFI/Plenum, New York, 1979).
[65] K. Negita, Acta Metall. **37**, 313 (1989).
[66] K. Negita and H. Takao, J. Phys. Chem. Solids **50**, 325 (1989).
[67] Y. Ishibashi and V. Dvořak, J. Phys. Soc. Jpn. **58**, 4211 (1989).
[68] *Phase Diagrams for Zirconium and Zirconia Systems*, edited by H. M. Ondik and H. F. McMurdie (National Institute of Standards and Technology/American Ceramic Society, Columbus, Ohio, 1998).
[69] A. P. Mirgorodsky, M. B. Smirnov, and P. E. Quintard, J. Phys. Chem. Solids **60**, 985 (1999).
[70] D. W. Liu, C. H. Perry, A. A. Feinberg, and R. Currat, Phys. Rev. B **36**, 9212 (1987).
[71] P. Li, I.-Wei Chen, and J. E. Penner-Hahn, Phys. Rev. B **48**, 10074 (1993).
[72] J. Cai, C. Raptis, Y. S. Raptis, and E. Anastassakis, Phys. Rev. B **51**, 201 (1995).
[73] J. M. Calderon-Moreno and M. Yoshimura, Solid State Ionics **154-155**, 125 (2002).
[74] C. Pecharromán, M. Ocaña, and C. J. Serna, J. Appl. Phys. **80**, 3479 (1996).
[75] E. Fernández López, V. Sánchez Escribano, M. Panizza, M. M. Carnasciali, and G. Busca, J. Mater. Chem. **11**, 1891 (2001).
[76] R. N. Patil and E. C. Subbarao, Acta Crystallogr., Sect. A: Cryst. Phys., Diffr., Theor. Gen. Crystallogr. **26**, 535 (1970).
[77] E. C. Subbarao, H. S. Maiti, and K. K. Srivastava, Phys. Status Solidi A **21**, 9 (1974).
[78] F. Frey, H. Boysen, and T. Vogt, Acta Crystallogr., Sect. B: Struct. Sci. **46**, 724 (1990).
[79] G. R. Hugo and B. C. Muddle, Mater. Sci. Forum **56-58**, 357 (1990).
[80] H. Boysen, F. Frey, and T. Vogt, Acta Crystallogr., Sect. B: Struct. Sci. **47**, 881 (1991).
[81] G. Fadda, L. Truskinovsky, and G. Zanzotto, Phys. Rev. B **66**, 174107 (2002).
[82] A. P. Mirgorodsky, M. B. Smirnov, and P. E. Quintard, Phys. Rev. B **55**, 19 (1997).
[83] P. Bouvier and G. Lucazeau, J. Phys. Chem. Solids **61**, 569 (2000).
[84] S. Fabris, A. T. Paxton, and M. W. Finnis, Phys. Rev. B **61**, 6617 (2000).
[85] L. K. Dash, N. Vast, Ph. Baranek, M.-C. Cheynet, and L. Reining, Phys. Rev. B **70**, 245116 (2004).
[86] O. Ohtaka, S. Kume, and E. Ito, J. Am. Ceram. Soc. **73**, 744 (1990).
[87] O. Ohtaka, T. Yamanaka, S. Kume, E. Ito, and A. Navrotsky, J. Am. Ceram. Soc. **74**, 505 (1991).
[88] P. Aldebert and J.-P. Traverse, J. Am. Ceram. Soc. **68**, 34 (1985).
[89] R. N. Patil and E. C. Subbarao, J. Appl. Crystallogr. **2**, 281 (1969).
[90] S. M. Lang, J. Am. Ceram. Soc. **47**, 641 (1964).
[91] R. J. Ackermann, E. G. Rauh, and C. A. Alexander, High. Temp. Sci. **7**, 304 (1975).
[92] M. W. Chase, *NIST-JANAF Thermochemical Tables*, Journal of Physical Chemical Reference Data Monographs Vol. 9, 4th ed. (National Institute of Standards and Technology, Gaithesburg, Maryland, 1998).
[93] S. Chan, Y. Fang, M. H. Grinsditch, Z. Li, M. V. Nevitt, W. M. Robertson, and E. S. Zouboulis, J. Am. Ceram. Soc. **74**, 1742 (1991).
[94] G. Fadda, L. Truskinovsky, and G. Zanzotto, Phys. Rev. B **68**, 134106 (2003).